CIRP Annals - Manufacturing Technology 71 (2022) 321–324

Contents lists available at ScienceDirect

CIRP Annals - Manufacturing Technology

journal homepage: https://www.editorialmanager.com/CIRP/default.aspx

Receptance coupling substructure analysis and chatter frequency-informed machine learning for milling stability

Tony Schmitz[a,b,*], Aaron Cornelius[a], Jaydeep Karandikar[b], Christopher Tyler[b], Scott Smith (1)[b]

[a] Department of Mechanical, Aerospace, and Biomedical Engineering, University of Tennessee, Knoxville, Knoxville, TN 37996, United States of America
[b] Manufacturing Science Division, Oak Ridge National Laboratory, Oak Ridge, TN 37830, United States of America

ARTICLE INFO

Article history:
Available online 26 April 2022

Keywords:
Milling
Stability
Machine learning

ABSTRACT

This paper describes a milling stability identification approach that simultaneously considers: physics-based models for the tool tip frequency response functions and stability predictions; the binary result from a milling test (automatically labeled as stable or unstable based on frequency content); chatter frequency when an unstable result is obtained; and user risk tolerance. The algorithm applies probabilistic Bayesian machine learning with adaptive, parallelized Markov Chain Monte Carlo sampling to update the probability of stability with each milling test. The result is a robust solution for rapid convergence to optimized milling parameters for maximum metal removal rate using all available information.

1. Introduction

There have been multiple studies on the application of machine learning (ML) to machining stability. For example, Cherukuri et al. used an artificial neural network (ANN) to model turning stability [1]. Denkena et al. applied support vector machines and ANNs [2]. Bergmann and Reimer implemented Regularized Kernel Interpolation for a learning stability lobe diagram to enable autonomous online parameter optimization [3]. Data-driven methods, such as ANNs, generally require many data points to accurately learn the stability boundary, do not provide information on the underlying tool tip frequency response function (FRF) and cutting force model, and may identify local, rather than global, optimized parameters [4]. Bayesian ML methods, on the other hand, enable updating the initial probabilistic stability boundary (or the prior) with each cutting test. However, recent Bayesian ML efforts [5–6] have still required significant data because the priors have not been systematically defined and test conditions have not been selected to maximize learning.

This paper describes a Bayesian ML method that implements: physics-based models to predict the tool tip FRF and stability boundary; updating using binary test results (stable/unstable) and chatter frequency (if the test cut is unstable); and the user's risk preference. The ML model is implemented using Markov Chain Monte Carlo (MCMC) sampling. Subsequently, the paper offers four new contributions to the state of the art and prior work by the authors [7–9]. First, receptance coupling substructure analysis (RCSA) is used to predict the tool tip FRF, which is an input to the stability boundary calculation [10], and removes the need to measure each tool-holder in each spindle [11]. Second, both the binary test result and the measured chatter frequency are used for knowledge updating. Third, the user's risk preference is considered when selecting test points. Fourth, a parallelized and adaptive MCMC method is applied to predict the probabilistic stability boundary. Prior Bayesian learning work by the authors did not use the stability model for updating [8–9], did not use RCSA for establishing the prior, did not consider the chatter frequency for updating, or use the risk-based approach for test point selection [7]. The comprehensive approach described here enables rapid identification of optimal milling operating parameters that maximize metal removal rate (MRR).

2. Defining the prior and probabilistic stability map

The initial stability map distribution is referred to as the prior in Bayesian ML. The frequency-domain stability model [10] requires two inputs: a milling force model, composed of the specific cutting force coefficient, K_s, and force angle, β; and the tool tip FRF. The prior is calculated by considering uncertainties in both the cutting force model and the tool point FRF prediction using RCSA. In the RCSA approach, a simple geometry artifact is first mounted in the spindle and measured by tap testing. Second, the spindle-machine FRF is calculated by mathematically decoupling the artifact. Third, the tool and holder models are coupled to the spindle-machine FRF to predict the tool tip FRF [12]; see Fig. 1.

In RCSA, Eq. (1) is applied to determine the spindle-machine FRFs, where the frequency-dependent R_{ij} (component, lower case coordinates) and G_{ij} (assembly, upper case coordinates) FRF matrices are defined in Eq. (2). In Eq. (2), x/X is lateral displacement, f/F is a harmonic force, θ/Θ is rotation, and m/M is a harmonic moment (or couple). The tool tip FRF is predicted using Eq. (3), where the R_{11}, R_{12a}, R_{2a2a}, and R_{2a1} matrices are defined by the free-free boundary

This manuscript has been authored in part by UT-Battelle, LLC under Contract No. DE-AC05–00OR22725 with the DOE. The US Government retains and the publisher, by accepting the article for publication, acknowledges that the US Government retains a non-exclusive, paid-up, irrevocable, world-wide license to publish or reproduce the published form of this manuscript, or allow others to do so, for United States Government purposes. The DOE will provide public access to these results of federally sponsored research in accordance with the DOE Public Access Plan (http://energy.gov/downloads/doe-public-access-plan).

* Corresponding author at: University of Tennessee Knoxville College of Engineering: The University of Tennessee Knoxville Tickle College of Engineering, Mechanical, 1512 Middle Drive, 204A Dougherty Engineering Building, Knoxville, Tennessee 37996, United States.
E-mail address: tony.schmitz@utk.edu (T. Schmitz).

https://doi.org/10.1016/j.cirp.2022.03.020
0007-8506/

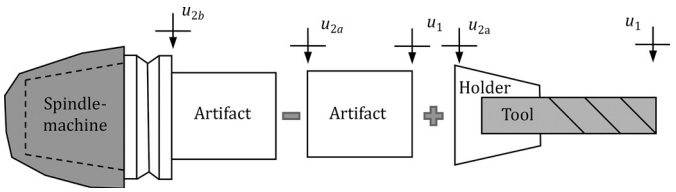

Fig. 1. Physics-based RCSA model for tool tip FRF prediction.

condition tool FRFs, R_{2b2b} represents a rigid connection of the spindle-machine and holder, the (1,1) location in the G_{11} matrix contains the required FRF for stability modeling, and the connection matrix, K, between the holder and tool is shown in Eq. (4), where k and c are stiffness and viscous damping and ω is the frequency. Uncertainty exists for k and c which gives uncertainty in the predicted tool tip FRF. Uncertainty also exists in the cutting force model. These uncertainties were used to calculate the initial probabilistic stability boundary.

$$R_{2b2b} = R_{2a1}(R_{11} - G_{11})^{-1}R_{12a} - R_{2a2a} \tag{1}$$

$$R_{ij} = \begin{bmatrix} \frac{x_i}{f_j} & \frac{x_i}{m_j} \\ \frac{\theta_i}{f_j} & \frac{\theta_i}{m_j} \end{bmatrix}, \; G_{ij} = \begin{bmatrix} \frac{X_i}{F_j} & \frac{X}{M_j} \\ \frac{\Theta_i}{F_j} & \frac{\Theta_i}{M_j} \end{bmatrix} \tag{2}$$

$$G_{11} = R_{11} - R_{12a}\left(R_{2a2a} + R_{2b2b} + \frac{1}{K}\right)^{-1} R_{2a1} \tag{3}$$

$$K = \begin{bmatrix} 0 & k + i\omega c \\ k + i\omega c & 0 \end{bmatrix} \tag{4}$$

Consider an application using a 12.7 mm diameter, three-flute endmill (Robbjack FMHV-304–16) clamped in a heat shrink holder (Haimer A63.140.1/2z.4) with a 65 mm tool stick out length and a 7050-T7451 aluminum work material. The tool and holder coupling uncertainty is modeled by uniform distributions: k = U(1×10^6, 1×10^7) N/rad and c = U(11, 20) N-s/rad, where U denotes a uniform distribution and the minimum and maximum values are listed. The uncertainty in k and c was propagated through the RCSA method using Monte Carlo simulation by sampling the distributions and predicting the FRF for each sampled pair. Fig. 2 (top left) shows 100 sample FRFs. Each FRF was fit with two vibration modes (natural frequency, f_n, modal stiffness, k, and modal damping ratio, ζ). The force model uncertainty is described using normal distributions: K_s = ℕ (600, 60) N/mm^2 and β = ℕ (68, 13.6) deg, where ℕ denotes a normal distribution and the mean and standard deviation are listed. For the two-mode dynamics, the set of input arguments is $\boldsymbol{\theta} = [K_S, \beta, f_{n_1}, k_1, \zeta_1, f_{n_2}, k_2, \zeta_2]$ for the stability model. The mean and covariance for the modal parameters

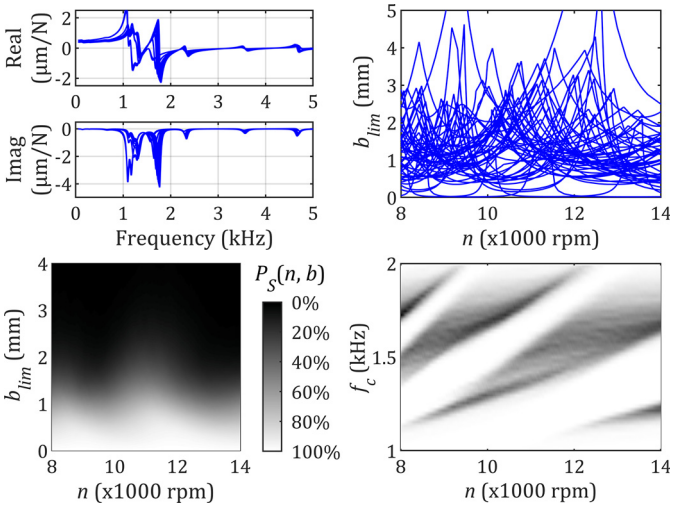

Fig. 2. (Top left) 100 sample FRF predictions with coupling parameter uncertainty. (Top right) 50 stability boundaries with FRF and cutting force model uncertainties. (Bottom left) Probabilistic stability map calculated using 4000 stability boundaries. (Bottom right) Chatter frequency distribution, where darker indicates more likely n-f_c pairs.

and the cutting force model terms were used to calculate the multivariate normal prior parameters distribution, $P_{prior}(\boldsymbol{\theta}) = N_d(\mu, S)$, where d is the number of dimensions, μ is the mean, and S is the covariance. A uniform distribution was selected for the coupling parameters to reflect higher uncertainty. A normal distribution was selected for the force model parameters based on author experience. In general, the prior distribution is selected based on all available information and user beliefs.

The FRF and cutting force model uncertainties were propagated through the stability model [10] using Monte Carlo simulation to calculate the initial probabilistic stability boundary. Fig. 2 (top right) shows 50 sample stability boundaries. Fig. 2 (bottom left) shows the probability of stability, P_s, as a function of the spindle speed, n, and axial depth of cut, b, calculated using 4000 sample stability boundaries. The probability of stability is the percentage of stability boundaries that predict a selected (n, b) pair is stable. Fig. 2 (bottom right) displays the chatter frequency, f_c, distribution from Monte Carlo simulation, where the gray scale identifies the probability density function, PDF, values and darker denotes higher probability for the n-f_c pairs.

3. Test point selection and evaluation

The testing objective is to identify stable parameters that maximize MRR. The spindle speed and axial depth of cut for testing are chosen based on the maximum MRR for a given probability of stability contour, P_{test}, which is based on the user's risk preference. For example, the user may wish to test parameters where the MRR is maximum with a 50% probability of stability, P_{test} = 50%. This reflects a moderate risk tolerance. A lower P_{test} = 25% choice exhibits a higher risk of selecting unstable test parameters, but may provide faster convergence to the optimum (n, b) pair if the cut is stable. Fig. 3 demonstrates test point selections for three P_{test} values, where the MRR is calculated using 75% radial immersion for the 12.7 mm diameter endmill and a feed per tooth of 0.1 mm. In practice, each test cut result is evaluated using a frequency analysis of the audio signal recorded using a microphone [13]. Chatter is identified when significant content occurs at a frequency that does not coincide with the tooth passing frequency or its multiples. The data for each test, α, therefore contains: spindle speed, axial depth, a binary variable indicating whether the cut was stable, and if unstable, the chatter frequency.

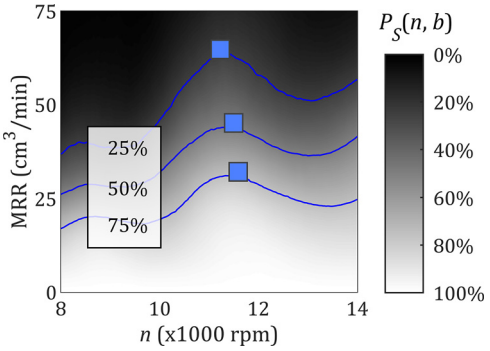

Fig. 3. Test selection based on risk tolerance. The blue lines show the MRR contours at 25%, 50%, and 75% probability of stability. The blue squares are the recommended test point for each risk tolerance, selected at the highest MRR for the corresponding P_{test} value.

4. Defining the posterior distribution

The test cut information is used to update the probability distribution by Bayes' rule. Each set of values, $\boldsymbol{\theta}$, sampled from the prior can be used to predict whether the test is stable and, if unstable, the chatter frequency using the stability algorithm. The closer $\boldsymbol{\theta}$ is to the true cutting force model and tool tip modal parameters, the more likely it is that it will correctly predict the results of the test cut. To account for uncertainty in the stability algorithm, the likelihood of observing the test results given the sample values and associated stability boundary, $P(\alpha|\boldsymbol{\theta})$, is calculated as a valuebetween 0 and 1. $P(\alpha|\boldsymbol{\theta})$ is determined by comparing the test result to the stability map predicted by $\boldsymbol{\theta}$ to find the

errors in stable cut depth, Δb, and predicted chatter frequency, Δf_c, using the following procedure (see Fig. 4):

- If the prediction is correct, then $\Delta b = 0$. Otherwise, Δb is the difference between the tested axial depth and the predicted limiting value, b_{lim}, at that spindle speed.
- If the cut was stable, there is no chatter frequency, so $\Delta f_c = 0$. If chatter occurs, Δf_c is the difference between the test and predicted frequencies.

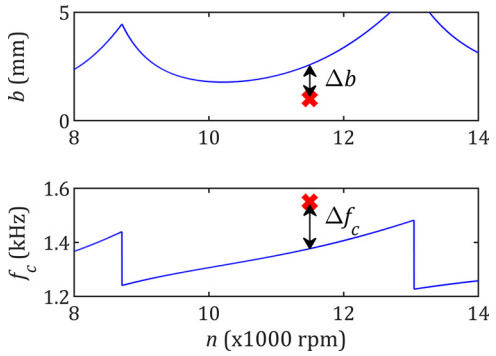

Fig. 4. Calculation of Δb and Δf_c for sample $\boldsymbol{\theta}$. (Top) Δb is the difference between the predicted limiting depth of cut, b_{lim} (line), and the unstable axial depth (×). (Bottom) Δf_c is the difference between the actual (×) and predicted (line) chatter frequencies.

Eq. (5) shows how Δb and Δf_c are applied to calculate the likelihood function $P(\alpha|\boldsymbol{\theta})$, where the user-selected parameters, σ_S and σ_{f_c}, specify the allowable disagreement in the stability boundary and chatter frequency. Larger values indicate larger allowable disagreement between the test and predicted values.

$$P(\alpha|\boldsymbol{\theta}) = \exp\left(-\frac{1}{2}\left(\left(\frac{\Delta b}{\sigma_S}\right)^2 + \left(\frac{\Delta f_c}{\sigma_{f_c}}\right)^2\right)\right) \tag{5}$$

$P(\alpha|\boldsymbol{\theta})$ is used to define a new distribution for $\boldsymbol{\theta}$ based on the test result using Bayes' rule; see Eq. (6). This new distribution, or posterior, considers both the original prior, $P_{prior}(\boldsymbol{\theta})$, and the new information obtained from the test cut. The posterior probability distribution after one update is used as the prior for the next. The posterior after n test cuts is shown in Eq. (7).

$$P(\boldsymbol{\theta}|\alpha) \propto P_{prior}(\boldsymbol{\theta}) \cdot P(\alpha|\boldsymbol{\theta}) \tag{6}$$

$$P(\boldsymbol{\theta}|\alpha_{1:n}) \propto P_{prior}(\boldsymbol{\theta}) \cdot \prod_{i=1}^{n} P(\alpha_i|\boldsymbol{\theta}) \tag{7}$$

The set of Monte Carlo samples is updated to approximate the posterior using rejection sampling. Here, $P(\alpha|\boldsymbol{\theta})$ is calculated for each sample (Eq. (5)) and the sample is randomly discarded with probability $1 - P(\alpha|\boldsymbol{\theta})$. The remaining samples, $\boldsymbol{\theta}^*$, approximate the posterior distribution, given by $P(\boldsymbol{\theta}|\alpha)$. Since samples are discarded with each update, the resulting stability map becomes less accurate as more tests are conducted. Therefore, an efficient method to draw new samples from the posterior is necessary.

5. MCMC sampling

MCMC methods are used to efficiently sample complex probability distributions and create a chain of samples that approximate the posterior. The size of each proposed step in the random walk procedure is determined by a preset proposal distribution and steps are accepted or rejected based on the ratio of the probability of the old and new positions on the chain [14]. However, MCMC algorithms have several challenges.

- The starting position for the random walk must be set in a high probability area or it will bias the MCMC chain.
- Manual parameter tuning may be needed to identify the most efficient proposal distribution.
- The sampling is completed serially since each step in the chain is dependent on the previous step.

A combination of rejection sampling and parallel adaptive MCMC overcomes these limitations. First, the starting location for MCMC is set using one of the retained samples from rejection sampling in $\boldsymbol{\theta}^*$, denoted by $\boldsymbol{\theta}_{last}$. As the retained samples are known to be in higher probability locations on the posterior, any may serve as a good starting position. Second, the proposal distribution is recalculated after every step using an adaptive MCMC method [14]. The proposal distribution is normal, $P_{\text{prop}} = \mathbb{N}(\boldsymbol{\theta}_{last}, 5.76/d \cdot \Sigma)$, where $\boldsymbol{\theta}_{last}$ is the last point on the current chain, Σ is the covariance matrix for all accepted samples, and d is the number of elements in the $\boldsymbol{\theta}$ vector [14]. Σ is calculated using both the current chain of samples and $\boldsymbol{\theta}^*$ to improve accuracy with the final posterior covariance. Third, the MCMC is parallelized to accept multiple points at each step [15]. For each step, j candidate samples, denoted by $\boldsymbol{\theta}^{cand}$, are drawn from P_{prop}. Then, k samples are drawn from the stationary distribution I formed by the candidates (note that $\boldsymbol{\theta}_0^{cand} = \boldsymbol{\theta}_{last}$).

$$I\left(\boldsymbol{\theta}_i^{cand}\right) = \frac{P(\boldsymbol{\theta}_i^{cand}|\alpha_{1:n})}{\sum_{l=0}^{j} P(\boldsymbol{\theta}_l^{cand}|\alpha_{1:n})} \tag{8}$$

The following steps are followed in the MCMC updating process.

1. Filter the prior samples with rejection sampling to obtain $\boldsymbol{\theta}^*$.
2. Calculate P_{prop} using the adaptive proposal algorithm [14].
3. Draw j candidate samples from P_{prop}, then accept k samples using Eq. (8) and append them to the output chain.
4. Repeat steps 2 and 3 until s unique samples are accepted.

This procedure is computationally efficient. For $j = k = 60$, $s = 4000$, the full sampling procedure is completed in ~45 s using an Intel i7−10750H CPU. Fig. 5 compares the posterior stability maps for stable and unstable cutting test and shows the subsequent selection of test points using P_{test} = 50%.

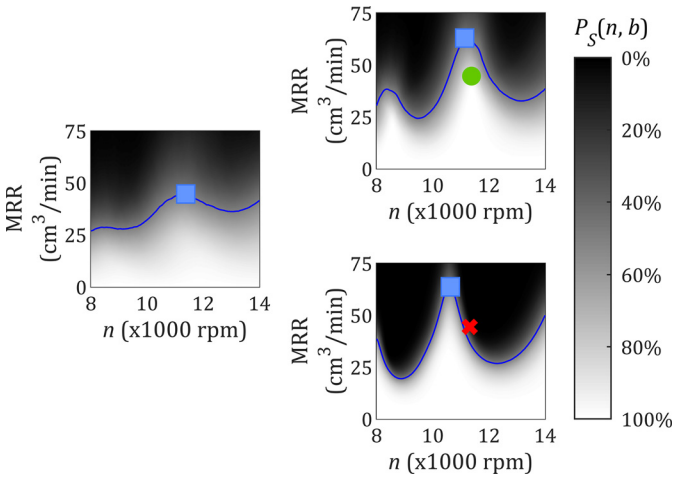

Fig. 5. MRR map updating. (Left) Test cut for maximized MRR with user risk preference. (Right) Updated posterior map if the test is stable (top) or unstable (bottom). In each map, the blue square is the next test cut.

6. Experimental setup and testing

Stability tests were completed to evaluate the Bayesian ML method using a DMG Mori Ultrasonic 65 machining center. As noted in Section 2, a 12.7 mm diameter, three-flute diameter endmill was clamped in a heat shrink holder and the work material was 7050-T7451 aluminum. The radial immersion was 75%, the feed was 0.1 mm/tooth, and flood coolant was applied. A directional microphone inside the machine enclosure was used to record the audio signal. The prior for this setup was defined in Fig. 2. The test cut selection and evaluation were completed using the Section 3 approach with P_{test} = 50%. The posterior stability distribution was calculated using the MCMC procedure described in Section 5. The likelihood (Eq. (5)) was calculated using $\sigma_S = 0.125$ mm and $\sigma_{f_c} = 50$ Hz. Testing was continued until MRR improvement for the next test point was less than 10%.

Fig. 6 shows the results. After five tests, the best operating parameters were n = 10,985 rpm and b = 3.4 mm with MRR = 107 cm^3/min. Since the next proposed test cut at 10,955 rpm and 3.7 mm would have only improved MRR by 9%, testing was terminated. There was one unstable cut (test 3) with f_c = 1550 Hz. To demonstrate the effect of risk tolerance, tests were also completed with $P_{test} = 25\%$ (aggressive) and 75% (conservative). The 25% test set was terminated after five tests with MRR = 131 cm^3/min, 22% higher than the 50% tests. The second test cut was unstable. The 75% test set was terminated after seven tests with MRR = 86 cm^3/min and an unstable result at the sixth test.

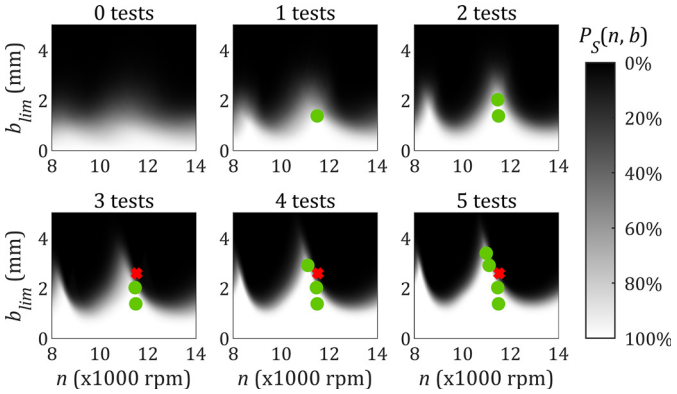

Fig. 6. Test sequence with $P_{test} = 50\%$.

Fig. 7 demonstrates the value of considering chatter frequency in the Bayesian updating. Without chatter frequency knowledge, stability boundaries with peaks to both the right (12,100 rpm) and left (11,200 rpm) of tests can predict the results (left panel). However, incorporating the 1550 Hz chatter frequency eliminates the stability boundaries with peaks at 12,100 rpm and improves the convergence to the true stability map (right panel). This is seen in the higher probability of stability at 11,200 rpm when considering the chatter frequency.

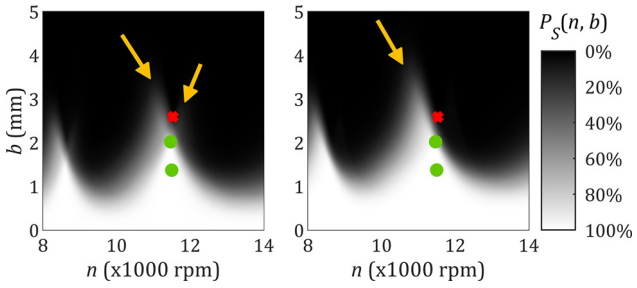

Fig. 7. Comparison of the posterior stability map after a test cut (left) without and (right) with chatter frequency knowledge. The arrows identify stability boundary peaks.

To validate the Bayesian ML algorithm performance in Fig. 6, a series of manually-selected tests were completed; see Fig. 8 The best parameters were n = 11,000 rpm and b = 3 mm with MRR = 94 cm^3/min, which is 28% lower than the best MRR identified by the Bayesian approach with $P_{test} = 25\%$.

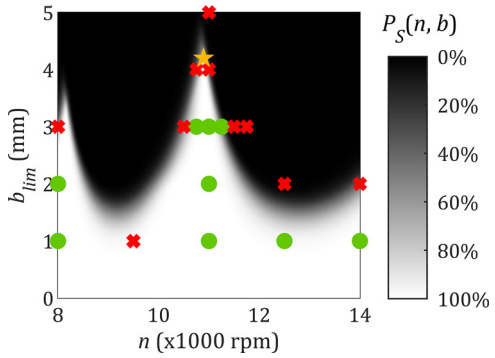

Fig. 8. Comparison of manually-selected tests to Bayesian ML method for $P_{test} = 25\%$. The star is the best operating parameters identified by the Bayesian method, while the other tests were manually selected.

7. Conclusions

This paper presented a Bayesian ML framework for identifying maximized MRR milling parameters. RCSA was used to establish an initial belief about the tool tip FRF, a key input to the stability map. The stability map was then updated, where the test selection was based on maximizing MRR while incorporating the user-specified risk preference. Experimental results show that the method can identify optimal milling parameters in a small number of test cuts and is computationally efficient. The effect of the user's risk preference was also explored. A higher risk tolerance helps to identify parameters with a higher MRR, but also tends to result in unstable cuts earlier in the testing process. Future research will focus on generalizing the method to more complex systems, such as those with asymmetric dynamics.

Declaration of Competing Interest

The authors declare that they have no known competing financial interests or personal relationships that could have appeared to influence the work reported in this paper.

Acknowledgment

This research was supported by the DOE Office of Energy Efficiency and Renewable Energy (EERE), Energy and Transportation Science Division, and used resources at the Manufacturing Demonstration Facility, a DOE EERE User Facility at Oak Ridge National Laboratory.

References

[1] Cherukuri H, Perez-Bernabeu E, Selles M, Schmitz T (2019) Machining chatter prediction using a data learning model. *J Manuf Mater* : 1–15. *Processing 3.2.45*.
[2] Denkena B, Bergmann B, Svenja R (2020) Analysis of different machine learning algorithms to learn stability lobe diagrams. *Procedia CIRP* 88:282–287.
[3] Bergmann B, Reimer S (2021) Online adaption of milling parameters for a stable and productive process. *CIRP Ann* : 341–344. *70.1*.
[4] Postel M, Bugdayci B, Wegener K (2020) Ensemble transfer learning for refining stability predictions in milling using experimental stability states. *Int J Adv Manuf Technol* : 4123–4139. *107.9*.
[5] Chen G, Li Y, Liu X, Yang B (2021) Physics-informed Bayesian inference for milling stability analysis. *Int J Mach Tools Manuf* 167:103767.
[6] Li K, He S, Liu H, Mao X, Li B, Bo L (2020) *Bayesian uncertainty quantification and propagation for prediction of milling stability lobe*, *Mechanical Systems and Signal Processing*, :106532.
[7] Cornelius A, Karandikar J, Gomez M, Schmitz T (2021) A Bayesian framework for milling stability prediction and reverse parameter identification. *Procedia Manuf* 53:760–772.
[8] Karandikar J, Honeycutt A, Schmitz T, Smith S (2020) Stability boundary and optimal operating parameter identification in milling using Bayesian learning. *J Manuf Process* 56:1252–1262.
[9] Karandikar J, Honeycutt A, Smith S, Schmitz T (2020) Milling stability identification using Bayesian machine learning. *Procedia CIRP* 93:1423–1428.
[10] Altintaş Y, Budak E (1995) Analytical prediction of stability lobes in milling. *CIRP Ann* : 357–362. *44.1*.
[11] Schmitz TL, Donaldson RR (2000) Predicting high-speed machining dynamics by substructure analysis. *CIRP Ann* : 303–308. *49.1*.
[12] Schmitz TL, Duncan GS (2005) Three-component receptance coupling substructure analysis for tool point dynamics prediction. *J Manuf Sci Eng* : 781–790. *127.4*.
[13] Smith S, Tlusty J (1992) Stabilizing chatter by automatic spindle speed regulation. *CIRP Ann* : 433–436. *41.1*.
[14] Haario H, Saksman E, Tamminen J (2001) An adaptive Metropolis algorithm. *Bernoulli* : 223–242.
[15] Calderhead B (2014) A general construction for parallelizing Metropolis-Hastings algorithms. In: *Proceedings of the National Academy of Sciences 111.49*, 17408–17413.